



Effective removal of Pb(II) and Cu(II) from aqueous solutions using a hybrid composite of fuller's earth, aluminum silicate and chitosan

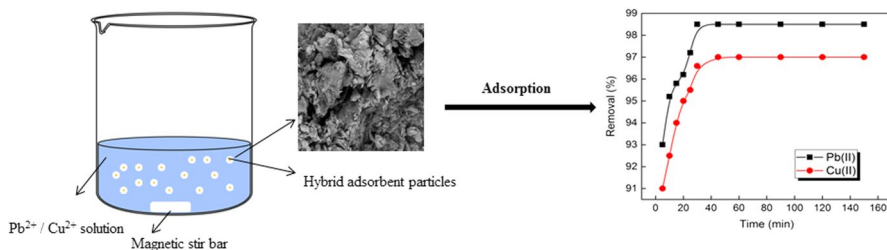
Heba Kandil¹ · Shaimaa T. El-Wakeel²

Received: 20 January 2023 / Revised: 28 March 2023 / Accepted: 29 March 2023
© The Author(s) 2023

Abstract

In this study, a highly effective hybrid adsorbent composite based on low-cost fuller's earth (FE), aluminum silicate (AS) and chitosan (CS) was prepared using a facile method. The prepared composite was applied to adsorb lead (Pb^{2+}) and copper (Cu^{2+}) ions from aqueous solutions. Several analyses such as Fourier transform infrared spectroscopy (FTIR), Scanning electron microscopy (SEM) and X-ray diffraction (XRD) were used to characterize the composite. The adsorption efficiency of the prepared composite was investigated at different operating conditions. Moreover, the adsorption isotherm/kinetic models and adsorption thermodynamics of the composite were examined. The results showed that the pseudo-second-order kinetic model described well with the obtained data and the adsorption equilibrium can be better described by Langmuir isotherm model with maximum adsorption capacities of 305.5 and 284.2 mg/g for Pb^{2+} and Cu^{2+} , respectively. The obtained data demonstrated that the prepared composite is an efficient and kinetically fast metal ion removal with high adsorption capacity and recovery efficiency.

Graphical abstract



Keywords Hybrid composite · Adsorption · Metal ions · Kinetic models · Isotherm models

Extended author information available on the last page of the article

Introduction

The deterioration of water quality that causes water pollution occurs mainly due to the recent rapid development of industrialization and urbanization [1–5]. Heavy metals are one of the toxic pollutants that primarily discharged to water resources from fertilizers, mining, tanneries and battery industries [3, 6]. These toxic metals are known to cause chronic poisoning and cancer risk due to their bioaccumulation in organisms [7–10].

Lead is one of the human toxic metals that can enter the body through inhalation and ingestion [11]. Lead accumulation in the bones, brain and kidney causes anemia, damages the nervous system and even death with long-term of exposure [12]. High concentrations of even necessary metals such as copper can also pose a threat to the environment [13]; its high accumulation causes headache, vomiting and respiratory problems, and excessive accumulation causes chronic liver injury [14]. There are several methods used for heavy metal removal such as chemical precipitation [15, 16], ion exchange [17], membrane separation [18], advanced oxidation processes [19, 20] and adsorption [21]. Among these methods, adsorption is considered the most favorable technique used to remove heavy metals over the other techniques because of its easy operation, simple design, low cost, high adsorption capacity and accessibility of various types of adsorbed materials [3, 7, 22]. Additionally, the adsorbent materials can be regenerated and reused, while the other methods have inherent limitations such as high energy consumption, high cost, sensitive operating conditions and the production of a large amount of sludge [23–25].

Many adsorbents have been used for heavy metal removal such as activated carbon [26], silica gel [27] and magnetite nanocomposites [28]. Due to the high cost of most of these materials, the need to study and develop low-cost adsorbent materials has increased [29]. Hence, special attention has recently been diverted toward the use of natural materials, agricultural waste and industrial waste as promising alternative adsorbents for the removal of metal ions, either in their natural form or after subjecting them to some modification [30–38].

Particular interest here was given to fuller's earth for its advantages over many other available adsorbent materials which included its low cost, non-toxic nature, high specific surface area and excellent adsorption properties [39, 40]. Fuller's earth is a naturally occurring sedimentary clay that consists of silicate, bentonite and a small proportion of magnesium as well as sodium [41]. However, being soft and easily crushing reduces its ability to be used as adsorbent [42]. Hence, it has been combined with other polymeric materials to produce composite materials that can be easily handled and separated within the adsorption process such as the beads prepared by Hasan et al. [42, 43] from combining fuller's earth with chitosan for use in removing cesium and strontium from waste stream and aqueous solutions, respectively. Kulkarni et al. [41] also prepared beads from combining fuller's earth with alginate to be used as an adsorbent for the removal of methylene blue (MB) dye from aqueous solutions. Hydrogel from fuller's earth (FE) was also prepared by Sharma et al. via incorporating FE into polyacrylamide

(PAAm)/cellulose (CG) hydrogel. The produced hydrogel was used for adsorption of MB dye [44]. In this study, fuller's earth was combined with chitosan and aluminum silicate to produce a promising hybrid composite for use in heavy metal ion removal. The hybrid composite was prepared using a facile method, characterized and applied for the removal of Pb(II) and Cu(II) ions from aqueous water. The kinetic/isotherm models of the composite were investigated to understand its adsorption mechanism. Additionally, its adsorbent reusability was investigated to determine its stability and potential recovery.

Materials and methods

Materials

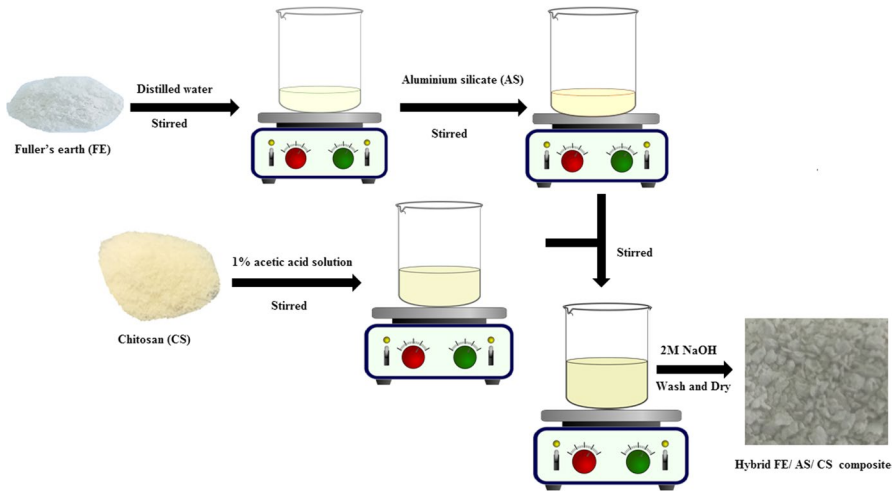
Chitosan (CS; degree of deacetylation is greater than > 75% with average molecular weight of 150 kDa) and acetic acid were provided from Sigma-Aldrich. Aluminum silicate Qp ($\text{Al}_2\text{O}_3 \cdot 2\text{SiO}_2 \cdot 2\text{H}_2\text{O}$) (AS) was supplied by Panreac Química SA. Fuller's earth LR (FE) was provided by Sd Fine Chem Limited Company. Sodium hydroxide (NaOH; 99%) was obtained from laboratory chemicals (modern lab). Lead nitrate and copper chloride of analytical grade were used for the preparation of stock solution containing 1000 mg/l of Pb(II) and Cu(II) and by its dilution different working solutions were prepared.

Preparation of hybrid fuller's earth/aluminum silicate/chitosan composite (FE/AS/CS)

To prepare the hybrid composite, fuller's earth (FE) was first mixed with AS where 1 g of aluminum silicate (AS) was added into 2 g of FE dispersed in 10 ml of distilled water. Then, the mixture solution was allowed to stir for 1 h till a complete dispersion of AS within FE solution. After that, the mixture solution was slowly added to a solution of 1 g of CS dissolved in 50 ml of 1% acetic acid solution. The obtained mixture was continuously stirred for 2 h till it became a homogeneous solution. After that, 100 ml of 2 M NaOH was slowly added to the solution as a white precipitate began to form. The resulting precipitate was left in NaOH solution overnight, then collected and washed with distilled water until the pH was neutral. Finally, the obtained precipitate (FE/AS/CS composite) was dried under vacuum at 60 °C for 24 h. Scheme 1 shows the synthesis procedure of the hybrid FE/AS/CS composite. For comparison, a control adsorbent from CS was prepared using the same process for preparing the FE/AS/CS composite except for the step of adding AS and FE.

Characterization

The functional groups of the prepared adsorbents were characterized using Fourier transform infrared (FTIR) spectrophotometer (Shimadzu 8400, Japan) with KBr disks. The morphologies of the prepared adsorbents were investigated using



Scheme 1 Procedure for the synthesis of FE/AS/CS composite

scanning electronic microscopy (SEM, Quanta FEG-250). The phase composition of the prepared adsorbents was studied using an X-ray diffractometer (XRD, Bruker AXS D8 advance instrument) of 2θ between 5 and 80° .

The point of zero charge pH_{ZPC} was determined using pH drift method for the prepared composite as follows: 0.15 g of adsorbent was added to solutions of 50 mL of 0.01 mol/l sodium chloride (NaCl), with different pH values (between 2 and 12) by adjusting with 0.1 mol/l hydrochloric acid (HCl) and 0.1 mol/l NaOH. Then, the mixtures were shaken for 48 h at room temperature [33, 34, 45–47]. The final solution pH values were measured, and the obtained data were curved versus the initial pH to obtain the point of intersection which expresses the pH_{PZC} value.

Batch adsorption experiments

The metal adsorption was conducted in batch mode at room temperature in a 50-mL conical flask containing the tested Pb(II) and Cu(II) ions. Based on the effects of different process variables on Pb(II) and Cu(II) adsorption, the following parameters were evaluated:

1. Contact time at different time intervals (5–150 min) using initial Pb(II) and Cu(II) concentrations of 10 mg/l with 0.5 g/l of adsorbent dose.
2. Initial Pb(II) and Cu(II) concentrations at 5, 10 and 50 mg/l using and different contact time intervals (5–150 min) with 0.5 g/l of adsorbent dose.
3. Initial pH values at the range of 2.0–6 for Pb(II) ions and 2.0–5 for Cu(II) ions using metal concentrations of 10 mg/l at the optimum contact time.
4. Adsorbent doses which tested at the range of 0.05–2 g/l at the optimum contact time and pH.

5. Temperature range (313–353 K) was used to test metal ion removal at initial concentration of 10 mg/l and the optimum contact time and pH.

Samples were filtered with a filter membrane of a pore size of 0.45 μm. Samples were analyzed for Pb(II) and Cd(II) concentrations using inductively coupled plasma optical emission spectrometry (ICP-OES) (Agilent 5100).

The adsorption capacity (q_e) of the metal on the adsorbent was estimated via equation

$$q_e = \frac{C_i - C_e}{m} \times V \tag{1}$$

where q_e is the adsorption capacity in (mg/g), C_i and C_e (mg/l) are the initial and final metal ion concentrations, respectively, V (l) is the volume of the solution taken and m (g) is the mass of the adsorbent.

Adsorption kinetic and isotherm study

To understand the adsorption mechanism, adsorption kinetic was studied using different kinetic models [37, 48–53]. Pseudo-first-order (Eq. 2), pseudo-second-order (Eq. 3), Elovich (Eq. 4) and intra-particle diffusion models (Eq. 5) have been tested for the present adsorption systems. The equations are presented as follows:

$$q_t = q_e - \left(1 - e^{(-k_1 t)}\right) \tag{2}$$

$$q_t = \frac{K_2 q_e^2 t}{1 + k_2 q_e t} \tag{3}$$

$$q_t = \frac{1}{\beta} \ln(1 + \alpha \beta t) \tag{4}$$

$$q_t = k_p t^{1/2} + C \tag{5}$$

where q_t is the amount of adsorbed metal at equilibrium (mg/g) at time t , k_1 (min^{-1}) and k_2 (g/mg min) are the adsorption rate constants, C is the intercept and k_p is the intra-particle diffusion rate constant (mg/g $\text{min}^{1/2}$). Values of β (g/mg) and α (mg/g min) represent constants related to the surface coverage degree and chemisorption rate, respectively.

Three replicate experiments were performed; then, the mean and standard deviation of metal adsorption were calculated and fitted using Origin Pro 2016 version 9.3.226 software. In the applied Origin software, different statistical parameters such as relation coefficient (R^2), sum of squared estimate of errors (SSE) and Chi-square (χ^2) values were calculated and compared with the fitted models to find the best model applying data precision.

The basic adsorption isotherm models, Langmuir (Eq. 6), Freundlich (Eq. 7), Dubinin–Radushkevich (D–R) (Eq. 8) and Redlich–Peterson (Eq. 9), have been investigated to understand the adsorption behavior for metal ion removal at constant temperature.

$$q_e = K_F C_e^{1/n} \quad (6)$$

$$q_e = q_m K_L \frac{C_e}{1 + K_L C_e} \quad (7)$$

$$q_e = q_s e^{(-K_{DR} \epsilon^2)} \quad (8)$$

$$q_e = \frac{K_R C_e}{1 + a_R C_e^g} \quad (9)$$

K_L (l/mg) is the Langmuir equilibrium constant related to the affinity of adsorption sites and q_m (mg/g) represents the maximum theoretical monolayer adsorption capacity.

C_e (mg/l) is the equilibrium concentration. k_F and n are the Freundlich adsorption constants which are related to the bonding energy and determine the deviation from the adsorption linearity. K_L (l/mg) is the Langmuir equilibrium constant related to the affinity of adsorption sites, and q_m (mg/g) represents the maximum concentration of adsorbed layer corresponding to monolayer. K_{DR} is a constant related to mean free energy (mol^2/kJ^2), q_s (mg/g) is related to the adsorption capacity and ϵ represents the Polanyi potential, which can be calculated from equation:

$$\epsilon = RT \ln \left(1 + \frac{1}{C_e} \right) \quad (10)$$

In Redlich–Peterson model, k_R (l/mg) is a constant related to the adsorption capacity, a_R (l/mg) is a constant related to the affinity of the binding sites and g exponent is related to the adsorption intensity which lies between 0 and 1.

Thermodynamics studies

The effect of temperature on the adsorption was studied at three different temperatures (303, 313 and 333 K). By this study, the change in Gibbs free energy (ΔG°), entropy (ΔS°) and enthalpy (ΔH°) could be determined according to the following equations:

$$\Delta G^\circ = -RT \ln K_d \quad (11)$$

$$\Delta G^\circ = \Delta H^\circ - T\Delta S^\circ \quad (12)$$

Desorption and regeneration study

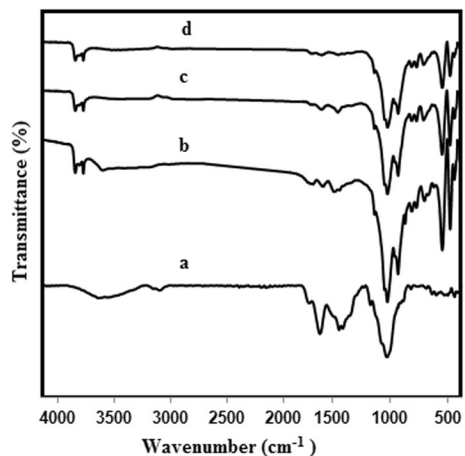
To study the metal desorption and the prepared composite reusability for metal ion adsorption, a number of adsorption–desorption cycles were performed. For metal desorption experiments, the metal ion-loaded composite samples were collected after adsorption experiment and then shaken with 0.1 M of HNO_3 which is used as an eluent to remove metal ions. The regenerated composite was rinsed with deionized water (DI) and then reused after drying for another cycle of adsorption. The concentrations of metal ions were measured at each step of process. To evaluate the reusability of the adsorbents, the regenerated composite was used for three successive adsorption/desorption recycles.

Result and discussion

Characterization of FE/AS/CS composite

Different analyses were used to characterize the FE/AS/CS composite such as FTIR, SEM and XRD. The FTIR spectra of FE/AS/CS composite and CS (control) adsorbents are shown in Fig. 1. By comparing the FTIR spectrum of CS with that of FE/AS/CS composite, it was observed that the characteristic vibration bands for CS were observed in both spectra besides the emergence of new bands in the spectrum of FE/AS/CS composite. The main characteristic bands of CS that were observed in both spectra were at 3393 cm^{-1} (for N–H and O–H stretching), 1573 cm^{-1} (due to N–H bending) and 1009 cm^{-1} (for C–O stretching) [54], while the new bands that were observed in the spectrum of FE/AS/CS composite were at 3688 cm^{-1} (for O–H stretching of Al–OH of FE and AS), 3619 cm^{-1} (for O–H stretching of structural hydroxyl groups of FE and AS), 910 cm^{-1} (due to Al–OH stretching of AS and FE), 848 cm^{-1} (for –OH bending of Al–Mg–OH of FE), 795 cm^{-1} (for Al–O stretching of FE and AS and Mg–O stretching of FE), and 529 and 461 cm^{-1} (for Si–O–Si and Si–O–Al bending of AS and FE)

Fig. 1 FTIR of **a** CS, **b** FE/AS/CS composite and **c**, **d** FE/AS/CS composite after Cu(II) and Pb(II) adsorption, respectively



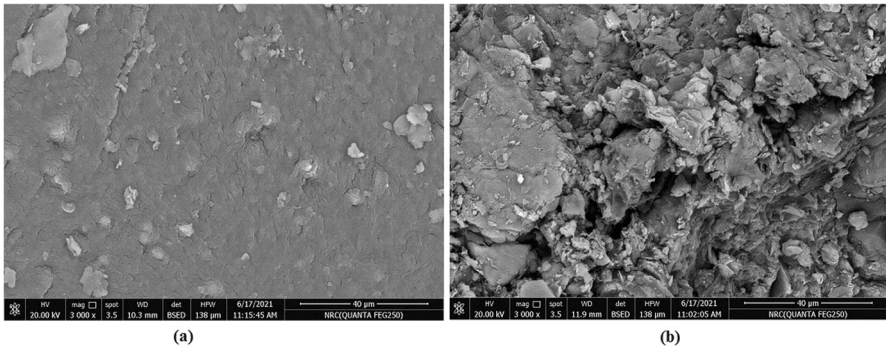


Fig. 2 SEM images of CS and FE/AS/CS composite adsorbents

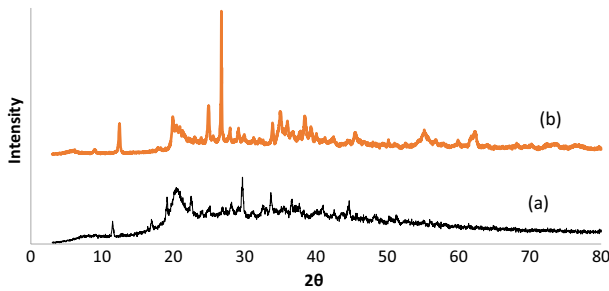


Fig. 3 XRD patterns of a CS and b FE/AS/CS composite

[55]. Since the characteristic vibration bands for CS, AS and FE were observed in the spectrum of FE/AS/CS composite, this indicates that the AS and FE were successfully combined with CS matrix.

Figure 2 shows SEM images of CS and FE/AS/CS composite adsorbents. It was found from the SEM image of FE/AS/CS composite that the surface morphology of the composite showed a rougher surface with irregular pores compared with the SEM image of the CS adsorbent. As a result of this roughness, this composite is expected to have a high adsorption capacity. This is attributed to the fact that the roughness provides more active sites for contaminant adsorption [56, 57].

In XRD pattern, peaks of chitosan (CS) are observed at $2\theta=20.4$ and 29.6° confirming the structure of CS (Fig. 3). In the prepared FE/AS/CS, the presence of FE, AS and CS was verified via peaks in the range $2\theta=15-40^\circ$. Peaks at 26.6° indicate the presence of FE and aluminum silicate, while CS peaks seem to be little shifted to 24.8° , suggesting that FE was well mixed with AS and CS.

Batch adsorption experiments for metal ions

The equilibrium time for maximum adsorption of Pb(II) and Cu(II) ions, on both CS and FE/AS/CS composite adsorbents, was investigated at different time intervals as shown in Fig. 4.

By using FE/AS/CS composite, the adsorption of both ions increased with time and was considered very rapid where the equilibrium was reached within 30 and 45 min with 98.5 and 97% removal for Pb(II) and Cu(II), respectively. Compared with the prepared FE/AS/CS composite, the prepared CS showed lower adsorption results for both metal ions showing removal (%) of 74 and 72% for Pb(II) and Cu(II) ions, respectively, after an hour of experiments. This result demonstrates the significant influence of fuller's earth and silicate. The increase in metal adsorption at the beginning of the adsorption is due to the presence of a large number of active sites which increase the adsorption of metal ions. The adsorption rate slowly increased until equilibrium was reached. After that, adsorption decreased. This decrease may be associated with a decrease in active sites.

The efficiency of adsorption was tested at different initial metal ion concentrations using 0.5 g/l of adsorbents at room temperature (Fig. 5). Metal ion adsorption decreased with the increase in initial concentration of metal ions for both adsorbents but no great difference in the removal was observed in the adsorption of metal ions of 5 and 10 mg/l. The possible reason could be that the driving force may overcome the resistance of adsorbate mass transfer from the bulk to the surface of the adsorbent [58]. The prepared composite still has a large adsorption ability for both tested metal ions using 50 mg/l of metal ions and the removal attained 92 and 90% for Pb(II) and Cu(II) ions, respectively, which reveals the efficiency of the prepared composite for metal ion adsorption at range of 5–50 mg/l.

Since the initial pH is one of the main factors affecting the adsorption process of heavy metals as it affects the solubility of metal ions, different values of pH are used to test metal ion removal. Using the prepared composite, it can be noticed that

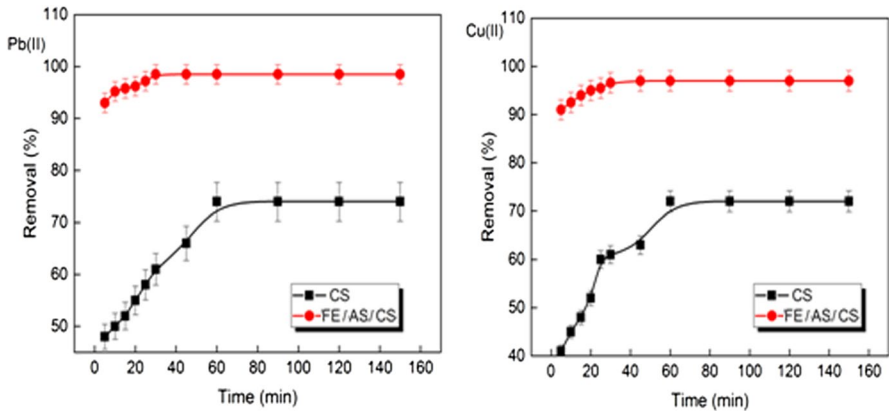


Fig. 4 Removal of Pb(II) and Cu(II) ions at different time intervals (dose 0.5 g/L; metal concentration 10 mg/l; agitation speed 200 rpm) by CS and FE/AS/CS composite

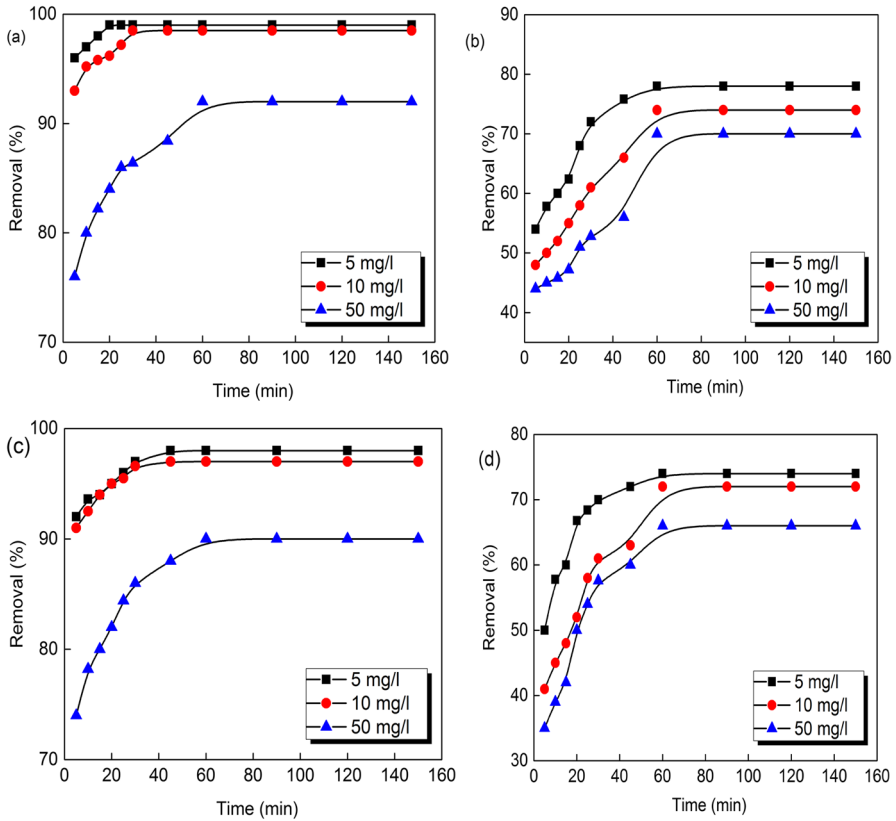
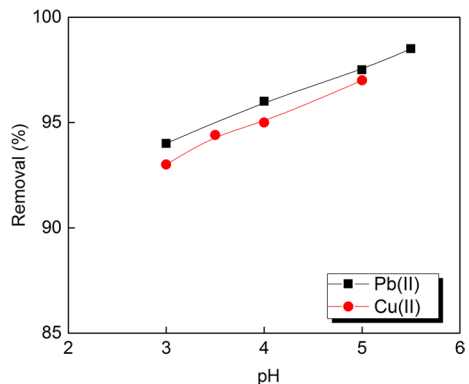


Fig. 5 Removal of Pb²⁺ and Cu²⁺ ions by: **a, c** FE/AS/CS composite and **b, d** CS, respectively, at different initial metal concentrations (amount of adsorbent 0.5 g/L; agitation speed 200 rpm)

with increasing pH, the removal of metal ions gradually increased and the maximum removal occurred at pH 5.5 and 5 for Pb(II) and Cu(II) ions, respectively (Fig. 6). Beyond pH values of 5.5 and 5 for Pb(II) and Cu(II), metal removal is a combination

Fig. 6 Removal of Pb²⁺ and Cu²⁺ ions by FE/AS/CS composite at different pH values (amount of adsorbent 0.5 g/L; initial metal concentration 10 mg/l)



of both adsorption and precipitation on the surface due to the formation of metal hydroxides. At low pH levels, the removal of metal ions by the composite was found to be low. This was due to the competition of hydrogen ions with the metal cations which reduced the adsorption [59].

The pH_{PZC} of the prepared composite was determined and found to be 4.2 (Fig. 7). It was shown that with increasing pH values above pH_{PZC} , the metal ion adsorption by the composite increased. This increase is because at $\text{pH} > \text{pH}_{\text{PZC}}$ the adsorbent surface becomes negative resulting in the formation of electrostatic attractions with positively charged metal ions. Whereas, at $\text{pH} < \text{pH}_{\text{PZC}}$, a decrease in the adsorption of metal ions by the composite occurred. This decrease is due to the presence of repulsion forces between the positively charged surface of the composite as a result of the richness of the solution with H^+ and the positively charged metal species [49]. So it is concluded that the adsorption of both metal ions is a combination of ion exchange. Similar findings were previously recorded for metal adsorption by different adsorbents [45, 49].

The adsorption efficiency of FE/AS/CS for metal ions was studied at different adsorbent doses of 0.05, 0.1, 0.5, 0.8, 1, 1.5 and 2 g/l at room temperature and initial metal concentration of 10 mg/l.

The adsorption capacity increased with the adsorbent dose for both ions up to 0.5 g/l where the maximum adsorption capacity was attained using both adsorbents, while there was a decrease in the adsorption capacity for both adsorbents, starting from the use of 1 g/L, which may have occurred due to the agglomeration of adsorbent particles and the occurrence of saturation of the active sites.

Adsorption kinetics and isotherm

To determine the rate determining mechanism of metal adsorption by the prepared composite, the adsorption kinetics were studied using the nonlinear fits of kinetic models as shown in equations [2–5]. The kinetic parameters were determined from models and the obtained data are summarized in Table 1.

By assuming the equilibrium conditions, the pseudo-first order (PFO) was applied in the nonlinear fits. It can be noticed that the reaction for both metal ions cannot be

Fig. 7 pH_{PZC} of the prepared FE/AS/CS composite

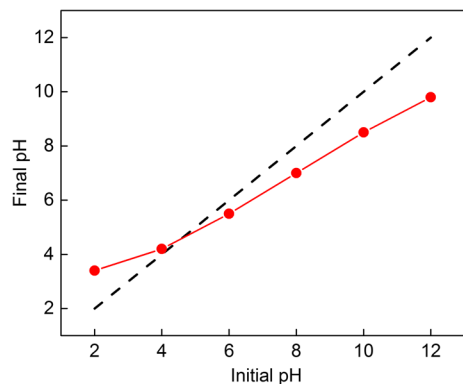


Table 1 Kinetic and isotherm parameters obtained for metal ion adsorption

| Metal | Pseudo-first order | | | | | |
|--------|--------------------------------|----------------------|---------|----------|----------|------|
| | $q_{e,exp.}$ (mg/g) | $q_{e,Cal}$ (mg/g) | K_1 | R^2 | χ^2 | RMSE |
| Pb(II) | 19.7 | 1.1 | 0.05 | 0.90 | 2.55 | 1.8 |
| Cu(II) | 19.4 | 1.3 | 0.09 | 0.90 | 3.2 | 2.1 |
| Metal | Pseudo-second order | | | | | |
| | $q_{e,Cal}$ (mg/g) | K_2 (g/mg min) | R^2 | χ^2 | RMSE | |
| Pb(II) | 20 | 0.125 | 0.99 | 0.01 | 1 | |
| Cu(II) | 19.6 | 0.09 | 0.99 | 0.09 | 1.3 | |
| Metal | Elovich | | | | | |
| | β (g/mg) | α (mg/g min) | R^2 | χ^2 | RMSE | |
| Pb(II) | 1.8 | 8.8×10^{14} | 0.80 | 5.52 | 2.5 | |
| Cu(II) | 1.4 | 4.4×10^{10} | 0.82 | 8.03 | 2.9 | |
| Metal | Langmuir isotherm parameters | | | | | |
| | q_m (mg/g) | K_L (L/mg) | R^2 | χ^2 | RMSE | |
| Pb(II) | 305.5 | 0.1 | 0.98 | 140.7 | 11.9 | |
| Cu(II) | 284.2 | 0.09 | 0.98 | 114.7 | 10.7 | |
| Metal | Freundlich isotherm parameters | | | | | |
| | $1/n$ | K_F (L/mg) | R^2 | χ^2 | RMSE | |
| Pb(II) | 0.27 | 75.9 | 0.97 | 265.5 | 16.3 | |
| Cu(II) | 0.25 | 71.7 | 0.96 | 317.4 | 17.8 | |
| Metal | D–R isotherm parameters | | | | | |
| | q_{K-D} (mg/g) | E (kJ/mol) | R^2 | χ^2 | RMSE | |
| Pb(II) | 264.4 | 13.38 | 0.94 | 1688.2 | 41 | |
| Cu(II) | 248.5 | 12.4 | 0.90 | 1093.03 | 33 | |
| Metal | Redlich–Peterson parameters | | | | | |
| | K_R (L/mg) | a_R (L/mg) | g (g) | R^2 | χ^2 | RMSE |
| Pb(II) | 46.5 | 0.27 | 0.88 | 0.96 | 180.1 | 13 |
| Cu(II) | 34.2 | 0.18 | 0.91 | 0.96 | 199.6 | 14 |

described well with this model because of the small values of correlation coefficient [$R^2 (< 0.96)$], besides that the values q_e calculated using the model were not matched to that determined experimentally.

On the other hand, the experimental data showed good fitting for the pseudo-second-order model (PSO) where the values of R^2 were larger ($R^2 > 0.96$) and the calculated q_e values using this model equation were matched to the experimental results for lead and copper ions. The PSO model assumed the variation of sites available

on the adsorbent surface with the adsorption rate, and by following the model, the chemical nature of the adsorption process was confirmed.

Elovich model is used to describe the chemisorption of gas onto the adsorbent, and this model assumes that the active adsorption sites of the adsorbent are heterogeneous [60]. Based on the obtained data (Table 1), it was found that R^2 values of Elovich model were lower than 0.96 and those of the pseudo-second-order equations for both metal ions. It is suggested that active adsorption sites of the adsorbent are homogeneous.

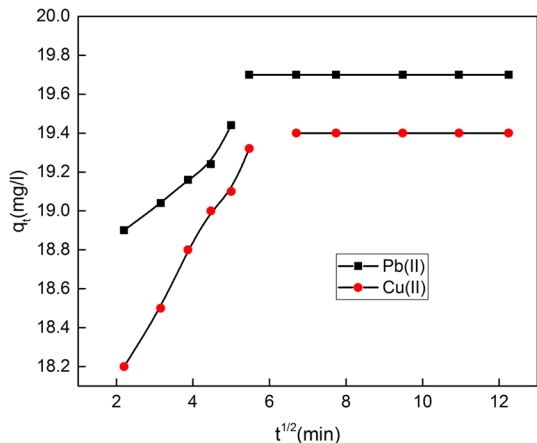
The adsorption model parameters and rate constants calculated from the plots are shown in Table 1. For more analysis of the rate determining step of the adsorption, the intra-particle diffusion model was applied to explain the transfer of metal ions from the solution to the adsorbent surface. In the adsorption process, metal ions in the boundary layer of adsorbent transfer to the surface of adsorbent (film diffusion). On the other hand, metal ions in the solute may transfer to the adsorbent sites (internal diffusion) or interact with the active sites on the adsorbent forming adsorption, precipitation or complexation. The model plot (Fig. 8) represents two adsorption stages: The first stage reveals the diffusion of metal ions to the adsorbent surface (film diffusion), while the second slow stage is attributed to the adsorption of ions into the adsorbent pores (internal diffusion process).

As shown in Fig. 8, the plot did not pass the origin and the obtained values of two intercepts C were not equal to zero which reveals that the intra-particle diffusion is not the only rate-controlling step but also the film diffusion that contributes to the sorption process.

The adsorption isotherm gives more information about the efficiency of the prepared adsorbent for the adsorption.

The adsorption of metal ions on the prepared composite was tested at different initial concentrations (25–250), and the obtained experimental data were fitted by the different nonlinear isotherm models. The plots are shown in Fig. 9, and the obtained parameters of the fitting are shown in Table 1.

Fig. 8 Intra-particle diffusion model for the adsorption of Pb(II) and Cu(II) by FE/AS/CS composite



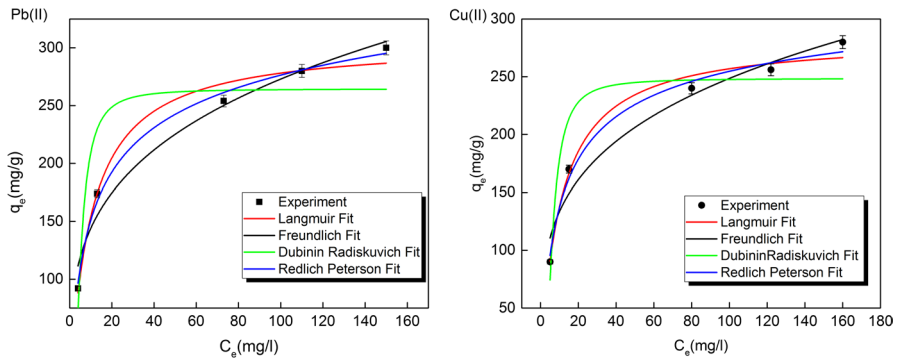


Fig. 9 Adsorption isotherm models of Pb(II) and Cu(II) adsorption by FE/AS/CS composite

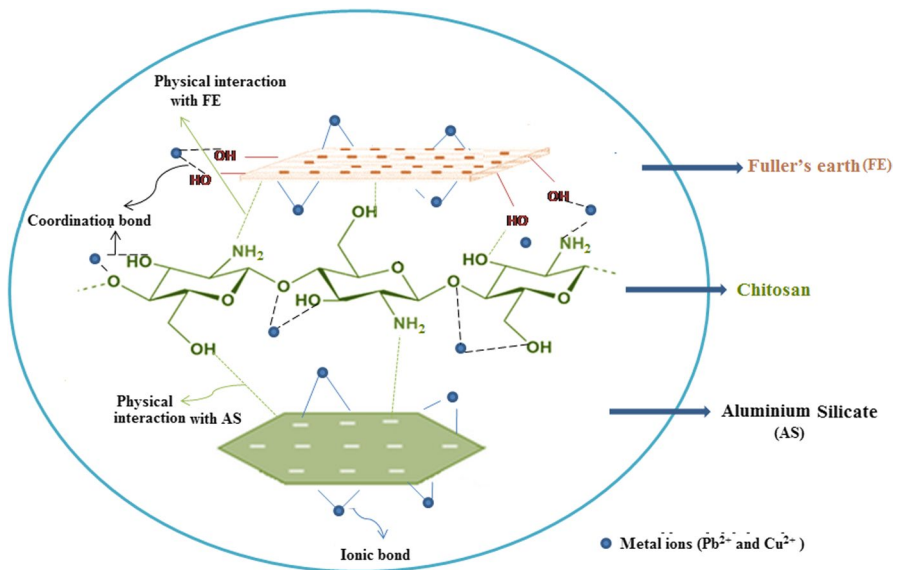


Fig. 10 Schematic diagram of the adsorption of Pb(II) and Cu(II) ions on the hybrid FE/AS/CS composite

The Freundlich model suggests the multilayer adsorption, while Langmuir model suggests that all sites are identical.

The plot in Fig. 9 shows good fit ($R^2=0.98$ and lowest Chi-square and RMSE values) with applying Langmuir adsorption isotherm model for the experimental data of both metal ions revealing the monolayer behavior of adsorption. In the model, the maximum adsorption capacities (q_m) were 312 and 294 mg/g for Pb^{2+} and Cu^{2+} , respectively.

The application of D–R isotherm on the experimental data showed less values of correlation coefficient (R^2) for both metal ions for the model that is based on the assumption of the filling adsorbent pores with solute.

The obtained E values were calculated as 13.3 and 12.2 kJ/mol for Pb^{2+} and Cu^{2+} , respectively. Values of E in the range of 8–16 kJ/mol reveal that the process is controlled by a chemical mechanism and occurs by ionic exchange or surface complexation [61]. The Redlich–Peterson isotherm model showed lower R^2 values than the other models, and it is a combination of the Langmuir and Freundlich isotherm models, applies inhomogeneous or heterogeneous surfaces and depends linearly on the concentration. Values of g in this model are $0 = g \leq 1$; when its value equals to 1, the model equation reduces to the Langmuir model, and while values equal to 0, it will reduce to Freundlich isotherm. As calculated from the study for g values, the model may reduce to the Langmuir model which estimated before to be the well-fitted model with the highest R^2 values.

Mechanism of adsorption Pb(II) and Cu(II) ions on the hybrid FE/AS/CS composite

The adsorption mechanism of the adsorption of metal ions with the prepared composite may be explained after the application of isotherm and kinetic models by that the surface can form surface complexes with divalent metal ions with the release of H^+ ions and the formation of AlO^- and SiO^- on the adsorbent surface.

The FTIR data obtained for the prepared composite confirmed the existence of many functional groups. After Pb(II) and Cu(II) adsorption, the FTIR spectra of FE/AS/CS (Fig. 1c, d) confirmed the interaction between heavy metal ions and composite, where a chemical shift was observed in the absorption peaks of certain functional groups as well as a clear reduction in their intensities as clearly seen in bands at 3688, 3619, 3452, 910, 848, 529 and 461 cm^{-1} . Figure 10 illustrates the proposed mechanism of adsorption Pb(II) and Cu(II) ions by the composite.

Comparison with other chitosan adsorbents

Numerous reports on the adsorption of Pb^{2+} and Cu^{2+} have been made by various materials based on chitosan. Hence, Table 2 presents a comparison of the q_m of FE/AS/CS with those of different adsorbents based on chitosan for the removal of Pb^{2+} and Cu^{2+} . The q_m of FE/AS/CS was found to be higher than those listed in Table 2. Therefore, it can be concluded that the FE/AS/CS is a promising adsorbent for the removal of Pb^{2+} and Cu^{2+} from aqueous solutions.

Thermodynamic studies

Thermodynamic parameters ΔG° , ΔS° and ΔH° for the analysis of the adsorption were determined from equations at 303, 313 and 333 K for both ions and the parameters value are listed in Table 3.

The estimated negative values of ΔG° revealed that the adsorption for Pb(II) and Cu(II) ions onto the prepared composite was spontaneous. The positive

Table 2 Comparison with different chitosan-based adsorbents for the removal of Pb²⁺ and Cu²⁺

| Adsorbent | Metal ions | q_m (mg/g) | References |
|---|------------------|--------------|------------|
| Chitosan/montmorillonite composite aerogel | Cu ²⁺ | 86.95 | [62] |
| Chitosan-coated PVC beads | Cu ²⁺ | 87.9 | [63] |
| Chitosan-coated gasifier biochar (CGBC) | Cu ²⁺ | 112 | [64] |
| Acrylic acid–chitosan blend hydrogel | Cu ²⁺ | 171 | [65] |
| Polyethylenimine (PEI)-modified polystyrene/Fe ₃ O ₄ /chitosan magnetic composite (PS/Fe ₃ O ₄ /CS-PEI) | Cu ²⁺ | 204 | [66] |
| Carboxymethyl chitosan–kaolinite composite hydrogel | Cu ²⁺ | 206 | [67] |
| Potato starch-graft-polyamidoxime embedded in chitosan beads | Cu ²⁺ | 238 | [68] |
| FE/AS/CS composite | Cu ²⁺ | 284.2 | This study |
| Magnetic chitosan/graphene oxide composites | Pb ²⁺ | 82.1 | [69] |
| Magnetic chitosan/anaerobic granular sludge composite | Pb ²⁺ | 97.97 | [70] |
| Branched polyethylenimine-enhanced magnetic carboxymethyl chitosan | Pb ²⁺ | 114.7 | [71] |
| Chitosan cross-linked with epichlorohydrin triphosphate | Pb ²⁺ | 166.94 | [72] |
| Acrylic acid–chitosan blend hydrogel | Pb ²⁺ | 192 | [65] |
| PEO/chitosan nanofiber membrane | Pb ²⁺ | 237.2 | [73] |
| FE/AS/CS composite | Pb ²⁺ | 305.5 | This study |

Table 3 Thermodynamic parameters for the adsorption of Pb(II) and Cu(II) ions onto the prepared composite

| Metal ions | ΔG° (kJ/mol) | | | ΔH° (kJ/mol) | ΔS° (J/mol·K) |
|------------|---------------------------|-------|-------|---------------------------|----------------------------|
| | 303 K | 313 K | 333 K | | |
| Pb(II) | -13.3 | -15.5 | -21 | 64.8 | 285.5 |
| Cu(II) | -10.9 | -11.9 | -14.3 | 23.6 | 113.9 |

value of ΔH° reveals that the adsorption was endothermic. The positive value of ΔS° reveals the randomness and disorganization between the solid and liquid surface and that the composite surface is preferential for Pb(II) and Cu(II) adsorption.

Reusability and regeneration

Adsorbents regeneration is important from the environmental and practical points of view and used to evaluate the efficiency of an adsorbent. For desorbing Pb(II) and Cu(II) ions, the HNO₃ solution (0.1 mol/L) was used and the results showed that the ions of Pb(II) and Cu(II) were recovered by 97 and 95.6%, respectively, after the third cycle revealing the good desorption ability for the tested metal ions. There was no obvious decline in the adsorption ability for

Pb(II) and Cu(II) on the prepared composite after the third successive adsorption/desorption cycles.

Conclusion

A hybrid composite of FE, AS and CS was successfully prepared using a facile method and was applied as adsorbent for heavy metal ions; Pb^{2+} and Cu^{2+} . Batch adsorption studies showed that the prepared composite had excellent efficiency in removing of Pb^{2+} and Cu^{2+} from aqueous solutions with maximum removals reaching 98.5 and 97 % for Pb^{2+} and Cu^{2+} , respectively. The adsorption process for both metal ions was fitted well with the Langmuir isotherm model, indicating that the chemical adsorption process was favorable and the rate determining step is not only controlled by intra-particle diffusion by applying intra-particle diffusion model. The reusability of the prepared composite indicated that it can keep its efficiency for the adsorption after the third cycle of adsorption/desorption. It can be concluded that the prepared composite can be used as an effective, eco-friendly, and low-cost adsorbent for lead and copper ions removal.

Author contributions The authors had equally contributed to conceptualization, methodology, formal analysis, software, writing the original draft, and reviewing and editing.

Funding Open access funding provided by The Science, Technology & Innovation Funding Authority (STDF) in cooperation with The Egyptian Knowledge Bank (EKB).

Declarations

Conflict of interest The authors declare no competing interests.

Open Access This article is licensed under a Creative Commons Attribution 4.0 International License, which permits use, sharing, adaptation, distribution and reproduction in any medium or format, as long as you give appropriate credit to the original author(s) and the source, provide a link to the Creative Commons licence, and indicate if changes were made. The images or other third party material in this article are included in the article's Creative Commons licence, unless indicated otherwise in a credit line to the material. If material is not included in the article's Creative Commons licence and your intended use is not permitted by statutory regulation or exceeds the permitted use, you will need to obtain permission directly from the copyright holder. To view a copy of this licence, visit <http://creativecommons.org/licenses/by/4.0/>.

References

1. Kandil H, Abdelhamid AE, Moghazy RM, Amin A (2022) Functionalized PVA film with good adsorption capacity for anionic dye. *Polym Eng Sci* 62:145–159
2. Fan Y, Fang C (2020) A comprehensive insight into water pollution and driving forces in Western China—case study of Qinghai. *J Clean Prod* 274:123950
3. Afroze S, Sen TK (2018) A review on heavy metal ions and dye adsorption from water by agricultural solid waste adsorbents. *Water Air Soil Pollut* 229:1–50

4. Teng Y, Yang J, Zuo R, Wang J (2011) Impact of urbanization and industrialization upon surface water quality: a pilot study of Panzhihua mining town. *J Earth Sci* 22(5):658–668
5. Mehdizadeh P, Jamdar M, Mahdi MA, Abdulsahib WK, Jasim LS, Yousefi SR, Salavati-Niasari M (2023) Rapid microwave fabrication of new nanocomposites based on Tb-Co-O nanostructures and their application as photocatalysts under UV/Visible light for removal of organic pollutants in water. *Arab J Chem* 16:104579
6. Ali H, Khan E, Ilahi I (2019) Environmental chemistry and ecotoxicology of hazardous heavy metals: environmental persistence, toxicity, and bioaccumulation. *J Chem* 2019:1–14
7. Wang J, Huyen Y, Yang Z, Zhang H, Zhang A, Kou X, Zhang Q, Zhang B (2019) Preparation of surface protein imprinted thermosensitive polymer monolithic column and its specific adsorption for BSA. *Talanta* 200:526–536
8. Wen J, Fang Y, Zeng G (2018) Progress and prospect of adsorptive removal of heavy metal ions from aqueous solution using metal–organic frameworks: a review of studies from the last decade. *Chemosphere* 201:627–643
9. Yousefi SR, Alshamsi HA, Amiri O, Salavati-Niasari M (2021) Synthesis, characterization and application of Co/Co₃O₄ nanocomposites as an effective photocatalyst for discoloration of organic dye contaminants in wastewater and antibacterial properties. *J Mol Liq* 337:116405
10. Yousefi SR, Sobhani A, Alshamsi HA, Salavati-Niasari M (2021) Green sonochemical synthesis of BaDy₂NiO₃/Dy₂O₃ and BaDy₂NiO₃/NiO nanocomposites in the presence of core almond as a capping agent and their application as photocatalysts for the removal of organic dyes in water. *RSC Adv* 11(19):11500–11512
11. Jaishankar M, Tseten T, Anbalagan N, Mathew BB, Beeregowda KN (2014) Toxicity, mechanism and health effects of some heavy metals. *Interdiscip Toxicol* 7:60
12. Kul AR, Koyuncu H (2010) Adsorption of Pb(II) ions from aqueous solution by native and activated bentonite: Kinetic, equilibrium and thermodynamic study. *J Hazard Mater* 179:332–339
13. He S, Zhang F, Cheng S, Wang W (2016) Synthesis of sodium acrylate and acrylamide copolymer/GO hydrogels and their effective adsorption for Pb²⁺ and Cd²⁺. *ACS Sustain Chem Eng* 4:3948–3959
14. Vardhan KH, Kumar PS, Panda RC (2019) A review on heavy metal pollution, toxicity and remedial measures: current trends and future perspectives. *J Mol Liq* 290:11197
15. Saleh TA, Mustaqeem M, Khaled M (2022) Water treatment technologies in removing heavy metal ions from wastewater: a review. *Environ Nanotechnol Monit Manag* 17:100617
16. Yousefi SR, Ghanbari M, Amiri O, Marzhoseyni Z, Mehdizadeh P, Hajizadeh-Oghaz M, Salavati-Niasari M (2021) Dy₂BaCuO₅/Ba₄DyCu₃O₉₋₀₉ S-scheme heterojunction nanocomposite with enhanced photocatalytic and antibacterial activities. *J Am Ceram Soc* 104:2952–2965
17. Vidu R, Matei E, Predescu AM, Alhalaili B, Pantilimon C, Tarcea C, Predescu C (2020) Removal of heavy metals from wastewaters: a challenge from current treatment methods to nanotechnology applications. *Toxics* 8(4):101
18. Qiu Y-R, Mao L-J (2013) Removal of heavy metal ions from aqueous solution by ultrafiltration assisted with copolymer of maleic acid and acrylic acid. *Desalination* 329:78–85
19. Du J, Zhang B, Li J, Lai B (2020) Decontamination of heavy metal complexes by advanced oxidation processes: a review. *Chin Chem Lett* 31(10):2575–2582
20. Yousefi SR, Ghanbari D, Salavati-Niasari M, Hassanpour M (2016) Photo-degradation of organic dyes: simple chemical synthesis of Ni(OH)₂ nanoparticles, Ni/Ni(OH)₂ and Ni/NiO magnetic nanocomposites. *J Mater Sci Mater Electron* 27:1244–1253
21. Guo C, Wang Y, Wang F, Wang Y (2021) Adsorption performance of amino functionalized magnetic molecular sieve adsorbent for effective removal of lead ion from aqueous solution. *Nanomaterials* 11:2353
22. Abdelhamid AE, Kandil H (2022) Facile approach to synthesis super-adsorptive hydrogel based on hyperbranched polymer for water remediation from methylene blue. *React Funct Polym* 177:105312
23. He J, Strezov V, Kumar R, Weldekidan H, Jahan S, Dastjerdi BH, Zhou X, Kan T (2019) Pyrolysis of heavy metal contaminated *Avicennia marina* biomass from phytoremediation: characterisation of biomass and pyrolysis products. *J Clean Prod* 234:1235–1245
24. Abu Taleb M, Halawani R, Neamtallah A, Kumar R, Barakat M (2022) Hybrid bioadsorbents for heavy metal decontamination from wastewater: a review. *Int J Eng Technol Innov* 2(1):5–19
25. Sud D, Mahajan G, Kaur MP (2008) Agricultural waste material as potential adsorbent for sequestering heavy metal ions from aqueous solutions—a review. *Bioresour Technol* 99(14):6017–6027

26. Sharma G, Naushad M (2020) Adsorptive removal of noxious cadmium ions from aqueous medium using activated carbon/zirconium oxide composite: isotherm and kinetic modelling. *J Mol Liq* 310:113025
27. Tzvetkova P, Nickolov R (2012) Modified and unmodified silica gel used for heavy metal ions removal from aqueous solutions. *J Chem Technol Metall* 47(5):498–504
28. Zhu Y, He X, Xu J, Fu Z, Wu S, Ni J, Hu B (2021) Insight into efficient removal of Cr (VI) by magnetite immobilized with *Lysinibacillus* sp. JLT12: mechanism and performance. *Chemosphere* 262:127901
29. Unuabonah EI, Günter C, Weber J, Lubahn S, Taubert A (2013) Hybrid clay: a new highly efficient adsorbent for water treatment. *ACS Sustain Chem Eng* 1(8):966–973
30. Sulyman M, Namiesnik J, Gierak A (2017) Low-cost adsorbents derived from agricultural by-products/wastes for enhancing contaminant uptakes from wastewater: a review. *Pol J Environ Stud* 26(3):479–510
31. Chowdhury IR, Chowdhury S, Mazumder MAJ, Al-Ahmed A (2022) Removal of lead ions (Pb²⁺) from water and wastewater: a review on the low-cost adsorbents. *Appl Water Sci* 12(8):185
32. Khera RA, Iqbal M, Ahmad A, Hassan SM, Nazir A, Kausar A, Khan MI (2020) Kinetics and equilibrium studies of copper, zinc, and nickel ions adsorptive removal on to *Archontophoenix alexandriae*: conditions optimization by RSM. *Desalin Water Treat* 201:289–300
33. Kuncoro EP, Soedarti T, Putranto TWC, Darmokoeseomo H, Abadi NR, Kusuma HS (2018) Characterization of a mixture of algae waste-bentonite used as adsorbent for the removal of Pb²⁺ from aqueous solution. *Data Brief* 16:908–913
34. Kuncoro EP, Isnadina DRM, Darmokoeseomo H, Fauziah OR, Kusuma HS (2018) Characterization, kinetic, and isotherm data for adsorption of Pb²⁺ from aqueous solution by adsorbent from mixture of bagasse-bentonite. *Data Brief* 16:622–629
35. Bhatnagar A, Minocha AK (2006) Conventional and non-conventional adsorbents for removal of pollutants from water—a review. *IJCT* 13:203–217
36. Chaemiso TD, Nefo T (2019) Removal methods of heavy metals from laboratory wastewater. *J Nat Sci Res* 9(2):36–42
37. Naat JN, Neolaka YA, Lapailaka T, Tj RT, Sabarudin A, Darmokoeseomo H, Kusuma HS (2021) Adsorption of Cu (II) and Pb (II) using silica@ mercapto (hs@ m) hybrid adsorbent synthesized from silica of Takari sand: optimization of parameters and kinetics. *Rasayan J Chem* 14(1):550–560
38. Neolaka YA, Riwu AA, Aigbe UO, Ukhurebor KE, Onyancha RB, Darmokoeseomo H, Kusuma HS (2022) Potential of activated carbon from various sources as a low-cost adsorbent to remove heavy metals and synthetic dyes. *Results Chem* 5:100711
39. Uddin MK (2017) A review on the adsorption of heavy metals by clay minerals, with special focus on the past decade. *Chem Eng J* 308:438–462
40. Zhang T, Wang W, Zhao Y, Bai H, Wen T, Kang S, Komarneni S (2021) Removal of heavy metals and dyes by clay-based adsorbents: from natural clays to 1D and 2D nano-composites. *Chem Eng J* 420:127574
41. Kulkarni P, Watwe V, Doltade T, Kulkarni S (2021) Fractal kinetics for sorption of methylene blue dye at the interface of Alginate Fullers earth composite beads. *J Mol Liq* 336:116225
42. Hasan S, Ghosh TK, Viswanath DS, Loyalka SK, Sengupta B (2007) Preparation and evaluation of fullers earth beads for removal of cesium from waste streams. *Sep Sci Technol* 42:717–738
43. Hasan S, Iasir ARM, Ghosh TK, Sen Gupta B, Prelas MA (2019) Characterization and adsorption behavior of strontium from aqueous solutions onto chitosan-fuller's earth beads. *Healthcare* 7:52
44. Sharma A, Pande PP, Khare P, Kumar K (2022) Synthesis and application of polyacrylamide/cellulose gel/fuller's earth composite for removal of methylene blue from water. *Iran J Chem Chem Eng* 41:3580
45. Neolaka YA, Supriyanto G, Darmokoeseomo H, Kusuma HS (2018) Characterization, isotherm, and thermodynamic data for selective adsorption of Cr (VI) from aqueous solution by Indonesia (Ende-Flores) natural zeolite Cr (VI)-imprinted-poly (4-VP-co-EGDMA)-ANZ (IIP-ANZ). *Data Brief* 17:1020–1029
46. Neolaka YA, Lawa Y, Naat J, Riwu AA, Lindu YE, Darmokoeseomo H, Widyaningrum BA, Iqbal M, Kusuma HS (2021) Evaluation of magnetic material IIP@ GO-Fe₃O₄ based on Kesambi wood (*Schleichera oleosa*) as a potential adsorbent for the removal of Cr (VI) from aqueous solutions. *React Funct Polym* 166:105000
47. Neolaka YA, Lawa Y, Naat J, Riwu AA, Mango AW, Darmokoeseomo H, Widyaningrum BA, Iqbal M, Kusuma HS (2022) Efficiency of activated natural zeolite-based magnetic composite (ANZ-Fe₃O₄) as a novel adsorbent for removal of Cr (VI) from wastewater. *J Mater Res Technol* 18:2896–2909

48. Neolaka YA, Lawa Y, Naat J, Lalang AC, Widyaningrum BA, Ngasu GF, Niga KA, Darmokoeseoemo H, Iqbal M, Kusuma HS (2023) Adsorption of methyl red from aqueous solution using Bali cow bones (*Bos javanicus domesticus*) hydrochar powder. *RINENG* 17:100824
49. Neolaka YA, Supriyanto G, Kusuma HS (2018) Adsorption performance of Cr (VI)-imprinted poly (4-VP-co-MMA) supported on activated Indonesia (Ende-Flores) natural zeolite structure for Cr (VI) removal from aqueous solution. *J Environ Chem Eng* 6:3436–3443
50. Neolaka YA, Lawa Y, Naat JN, Riwu AAP, Darmokoeseoemo H, Supriyanto G, Holdsworth CI, Amengahawon AN, Kusuma HS (2020) A Cr (VI)-imprinted-poly (4-VP-co-EGDMA) sorbent prepared using precipitation polymerization and its application for selective adsorptive removal and solid phase extraction of Cr (VI) ions from electroplating industrial wastewater. *React Funct Polym* 147:104451
51. Neolaka YA, Lawa Y, Naat JN, Riwu AA, Iqbal M, Darmokoeseoemo H, Kusuma HS (2020) The adsorption of Cr (VI) from water samples using graphene oxide-magnetic (GO-Fe₃O₄) synthesized from natural cellulose-based graphite (kusambi wood or *Schleichera oleosa*): study of kinetics, isotherms and thermodynamics. *J Mater Res Technol* 9:6544–6556
52. Budiana IGMN, Jasman J, Neolaka YA, Riwu AA, Elmsellem H, Darmokoeseoemo H, Kusuma HS (2021) Synthesis, characterization and application of cinnamoyl C-phenylcalix [4] resorcinarene (CCPCR) for removal of Cr (III) ion from the aquatic environment. *J Mol Liq* 324:114776
53. Mahreni M, Ramadhan RR, Pramadhana MF, Permatasari AP, Kurniawati D, Kusuma HS (2022) Synthesis of metal organic framework (MOF) based Ca-Alginate for adsorption of malachite green dye. *Polym Bull* 79:11301–11315
54. Kandil H, Ali H (2023) Simultaneous removal of cationic crystal violet and anionic reactive yellow dyes using eco-friendly chitosan functionalized by Talc and Cloisite 30B. *J Polym Environ* 31:1456–1477
55. Madejová JJ (2003) FTIR techniques in clay mineral studies. *Vib Spectrosc* 31(1):1
56. Kakavandi B, Raofi A, Peyghambarzadeh SM, Ramavandi B, Niri MH, Ahmadi M (2018) Efficient adsorption of cobalt on chemical modified activated carbon: characterization, optimization and modeling studies. *Desalin Water Treat* 111:310–321
57. Che H, Che G, Zhou P, Liu C, Dong H (2019) Yeast-derived carbon sphere as a bridge of charge carriers towards to enhanced photocatalytic activity of 2D/2D Cu₂WS₄/g-C₃N₄ heterojunction. *J Colloid Interface Sci* 546:262–275
58. Kandil H, Moghazy RM, Amin A (2023) Enhancing the adsorption affinity of cellulose acetate film toward cationic dye by incorporating Cloisite 30B grafted with polyacrylic acid. *Polym Eng Sci* 63:769–781
59. Gao X, Guo C, Hao J, Zhao Z, Long H, Li M (2020) Adsorption of heavy metal ions by sodium alginate based adsorbent—a review and new perspectives. *Int J Biol Macromol* 164:4423–4434
60. Li X, Wen B, Li Y (2017) Adsorption of the malachite green by magnetic clam shell powder. *Pol J Environ Stud* 30:717–726
61. Dada A, Olalekan A, Olatunya A, Dada O (2012) Langmuir, Freundlich, Temkin and Dubinin-Radushkevich isotherms studies of equilibrium sorption of Zn²⁺ unto phosphoric acid modified rice husk. *IOSR-JAC* 3:38–45
62. Ye X, Shang S, Zhao Y, Cui S, Zhong Y, Huang L (2021) Ultra-efficient copper ions adsorption of chitosan-montmorillonite composite aerogel for wastewater treatment. *Cellulose* 28:7201–7212
63. Popuri SR, Vijaya Y, Boddu VM, Abburi K (2009) Adsorptive removal of copper and nickel ions from water using chitosan coated PVC beads. *Bioresour Technol* 100:194–199
64. Burk GA, Herath A, Crisler GB, Bridges D, Patel S, Pittman CU Jr, Mlsna T (2020) Cadmium and copper removal from aqueous solutions using chitosan-coated gasifier biochar. *Front Environ Sci* 8:541203
65. Marjub MM, Rahman N, Dafader NC, Tuhen FS, Sultana S, Ahmed FT (2019) Acrylic acid-chitosan blend hydrogel: a novel polymer adsorbent for adsorption of lead (II) and copper (II) ions from wastewater. *J Polym Eng* 39:883–891
66. Xiao C, Liu X, Mao S, Zhang L, Lu J (2017) Sub-micron-sized polyethylenimine-modified polystyrene/Fe₃O₄/chitosan magnetic composites for the efficient and recyclable adsorption of Cu (II) ions. *Appl Surf Sci* 394:378–385
67. He G, Wang C, Cao J, Fan L, Zhao S, Chai Y (2019) Carboxymethyl chitosan-kaolinite composite hydrogel for efficient copper ions trapping. *J Environ Chem Eng* 7:102953
68. Dragan ES, Apopei Loghin DF, Cocarta AI (2014) Efficient sorption of Cu²⁺ by composite chelating sorbents based on potato starch-graft-polyamidoxime embedded in chitosan beads. *ACS Appl Mater Interfaces* 6:16577–16592
69. Fan L, Luo C, Sun M, Li X, Qiu H (2013) Highly selective adsorption of lead ions by water-dispersible magnetic chitosan/graphene oxide composites. *Colloids Surf B Biointerfaces* 103:523–529

70. Liu T, Han X, Wang Y, Yan L, Du B, Wei Q, Wei D (2017) Magnetic chitosan/anaerobic granular sludge composite: synthesis, characterization and application in heavy metal ions removal. *J Colloid Interface Sci* 508:405–414
71. Wang Y, Wu D, Wei Q, Wei D, Yan T, Yan L, Hu L, Du B (2017) Rapid removal of Pb (II) from aqueous solution using branched polyethylenimine enhanced magnetic carboxymethyl chitosan optimized with response surface methodology. *Sci Rep* 7:1–11
72. Laus R, Costa TG, Szpoganicz B, Fávere VT (2010) Adsorption and desorption of Cu (II), Cd (II) and Pb (II) ions using chitosan crosslinked with epichlorohydrin-triphosphate as the adsorbent. *J Hazard Mater* 183:233–241
73. Aliabadi M, Irani M, Ismaeili J, Piri H, Parnian MJ (2013) Electrospun nanofiber membrane of PEO/Chitosan for the adsorption of nickel, cadmium, lead and copper ions from aqueous solution. *Chem Eng J* 220:237–243

Publisher's Note Springer Nature remains neutral with regard to jurisdictional claims in published maps and institutional affiliations.

Authors and Affiliations

Heba Kandil¹  · Shaimaa T. El-Wakeel²

✉ Heba Kandil
heba_saladin@yahoo.com

¹ Polymers and Pigments Department, National Research Centre, 33 El Buhouth St., Dokki, Giza 12622, Egypt

² Water Pollution Research Department, National Research Centre, 33 El Buhouth St, Dokki, Giza 12622, Egypt